

# Mixed Hyperbranched/Triblock Copolymer Micelle Assemblies: Physicochemical Properties and Potential for Drug Encapsulation

Angelica Maria Gerardos, Anastasia Balafouti, and Stergios Pispas\*

Mixed micelles have numerous advantages while requiring little to no effort in preparation. This study aims to produce mixed micelle nanostructures from a linear triblock copolymer and a hyperbranched random copolymer, and is able to be loaded with the weakly water-soluble drugs curcumin and indomethacin. Different preparation techniques are employed to produce mixed micelles comprised of Pluronic F127 block copolymer, and hyperbranched poly[(ethylene glycol) methyl ether methacrylate-co-lauryl methacrylate], H-[P(OEGMA-co-LMA)], copolymer. Few studies have dabbled in these types of coassemblies, which provides insight into how structural differences of each copolymer can affect the formation of micelles. To determine the properties of the emerging nanostructures in aqueous environments, including their size, homogeneity, and surface charge, different physicochemical techniques are used, such as light scattering and spectroscopic methods. The results reveal that the copolymers combine, and spontaneously self-assemble into mixed micelle-like nanostructures in aqueous environments, whereas both systems of neat and drug-loaded nanostructures exhibit desirable properties such as small average micelle hydrodynamic radii and low size polydispersity indices. The nanostructures that result from the effective encapsulation of curcumin exhibit outstanding stability over 169 days. The fluorescent qualities of curcumin persist after encapsulation, making the novel nanostructures excellent candidates for bioimaging applications.

in place to make these compounds bioavailable to prevent missing out on attractive therapeutic prospects.<sup>[1,2]</sup> Excipients such as polymeric micelles may therefore be able to aid with this challenge. These vehicles are primarily composed of two parts: a lipophilic core that acts as a micro reservoir for the encapsulation of hydrophobic drugs and a hydrophilic shell that, when exposed, can interact with the biological environment to safeguard the therapeutic cargo.<sup>[3,4]</sup> Often when compared to other amphiphilic nanocarriers, such as liposomes, polymeric micelles have great advantages due to their significant solubilization ability, larger encapsulation efficiency, and superior circulatory integrity. The nanocarriers' size permits passive accumulation in areas with enhanced permeability, such as tumors and inflammatory regions, due to the enhanced permeability and retention (EPR) effect, while inhibiting rapid renal elimination. These types of nanostructures can be designed to break down into their parent copolymers in reaction to external stimuli. Once their payload is released, this process begins and ends with renal excretion, without lasting adverse effects.<sup>[5-7]</sup>

Curcumin is the most abundant polyphenolic component in turmeric. It is derived from the rhizome of turmeric, a perennial plant known scientifically as *Curcuma longa*. Asian nations have historically used turmeric in medicine. Researchers have thoroughly explored the potential of curcumin in light of this. Numerous therapeutic possibilities, spanning anti-inflammatory, anti-tumor, anti-microbial, anti-protein aggregation, and wound healing properties, have been explored. Curcumin is a fluorescent hydrophobic molecule. Considering chemical structure, based on the pH, curcumin undergoes keto-enol tautomerization, which produces two isomers. The stable enolic form predominates in alkaline conditions, while the keto form is favored at pH levels  $\leq 7$ . In physiological conditions, curcumin has been observed to rapidly break down into substances like vanillin and ferulic acid.<sup>[8-13]</sup> Curcumin is most stable in acidic environments, while its water solubility is low in these conditions. On the other hand, in an alkaline medium, curcumin solubility is increased although degradation is rapid.<sup>[14,15]</sup> Numerous research studies have shown

## 1. Introduction

Lipophilic drug candidates are becoming increasingly common in drug research. Innovative formulation strategies must be put

A. M. Gerardos, A. Balafouti, S. Pispas  
 Theoretical and Physical Chemistry Institute  
 National Hellenic Research Foundation  
 48 Vassileos Constantinou Avenue, Athens 11635, Greece  
 E-mail: pispas@eie.gr

 The ORCID identification number(s) for the author(s) of this article can be found under <https://doi.org/10.1002/macp.202300109>

© 2023 The Authors. Macromolecular Chemistry and Physics published by Wiley-VCH GmbH. This is an open access article under the terms of the Creative Commons Attribution-NonCommercial License, which permits use, distribution and reproduction in any medium, provided the original work is properly cited and is not used for commercial purposes.

DOI: 10.1002/macp.202300109

that following oral administration, insignificant amounts of curcumin were detectable in serum.<sup>[16,17]</sup> As a result of the aforementioned, new excipients are needed to address these significant challenges.

Indomethacin is a highly effective nonsteroidal anti-inflammatory drug (NSAID). Symptoms like headache, fever, edema, stiffness, and discomfort in joints are commonly treated with this moderately hydrophobic drug. These characteristics make indomethacin an essential component in the treatment of connective tissue diseases, osteoarthritis, rheumatoid arthritis, tendinitis, chronic migraines, and menstrual cramps. Indomethacin operates by inhibiting the cyclooxygenase enzymes (COX-1 and COX-2) in the conversion of arachidonic acid, hence restricting prostaglandin synthesis in the tissues. This drug is associated with some adverse reactions, including indomethacin-induced gastric ulcers after oral administration and central nervous system toxicity (e.g., confusion), and renal toxicity as an inevitable result of high blood levels. This is because maintaining the gastric mucosa from irritation necessitates the production of prostaglandins. When administering this medication as prescribed, these side effects occur in 30 to 60% of patients, and 10 to 20% of them terminate treatment as a result.<sup>[18–25]</sup> Since passive targeting minimizes the drug's availability in the bloodstream, it is expected that nanoencapsulation may lessen the aforementioned effects.

Polymeric micelles which are derived from one type of copolymer may exhibit insufficiency in certain aspects, given that these micelles are hampered by the fact that they possess a limited quantity of building blocks. Pairing various amphiphilic polymers to create mixed micelles is an established but less explored strategy for overcoming these challenges. There is the potential to improve the present optimal features and eliminate some of the emerging drawbacks of conventional polymeric micelles with ease in terms of synthetic techniques. Research has repeatedly demonstrated that mixed micelles could offer significant benefits by improving micelle stability and drug encapsulation efficiency.<sup>[10,26–28]</sup>

Hyperbranched polymers are widely thought of as dendrimer imperfect analogs. The production of dendrimers on a wide scale can be prohibitively expensive for many applications. On the other hand, the one-pot simple synthesis that results in hyperbranched copolymers with a similar structure to dendrimers is of major value to both research and commercial applications. In contrast to their linear counterparts, hyperbranched polymers exhibit excellent functionality, greater segment density, and superior solubility. The abundance of functional groups also makes it possible to optimize many parameters including size, solubility, biocompatibility, and loading capacity.<sup>[29–34]</sup> Considering the fact curcumin has previously been successfully encapsulated in earlier studies using H-[P(OEGMA-co-LMA)] copolymers, H-[P(OEGMA-co-LMA)] 50% wt LMA was selected as the random hyperbranched copolymer to examine the preparation of mixed micelles from copolymers with varying architecture and topology. In brief, divinyl monomer ethylene glycol dimethacrylate (EGDMA) was employed as the branching agent, while OEGMA with an average  $M_n = 950 \text{ g mol}^{-1}$  was specifi-

cally chosen to offer superior water solubility. In accordance with its compatibility with methacrylic monomers, 4-cyano-4-(phenylcarbonothioylthio)pentanoic acid (CPAD) was utilized as the chain transfer agent.<sup>[35]</sup> Both OEGMA and LMA are commonly available monomers. OEGMA provides a hydrophilic character to the system. Multiple ethylene oxide (EO) units connected across a hydrophobic methyl methacrylate chain are responsible for POEGMA's hydrophilicity.<sup>[36]</sup> Notably, a number of recent studies discovered that nonlinear PEG analogs, such as POEGMA, are just as nonimmunogenic as their linear equivalents.<sup>[37]</sup> LMA provides a hydrophobic character to the structure due to the long hydrocarbon side chain group, which also can offer systems high flexibility.<sup>[38]</sup>

Thermosensitive polymers have attracted considerable scientific interest, these smart polymers have the potential to be widely used for controlled drug release applications. A well-designed controlled drug delivery system can deliver the correct dose of a drug to a specific area of the body in a controlled manner. It is feasible to deliver the drug as a liquid that gels when exposed to body temperature using these polymers.<sup>[39–41]</sup> This is brought on by the transition at the lower critical solution temperature (LCST). When exposed to an aqueous environment, such polymers below this value are water-soluble because hydrogen bonds occur among water molecules and the polymer chains. When the temperature rises above this point, the intermolecular bonds are weakened, causing the polymer to become hydrophobic which can lead it to break down or precipitate. Pluronics are a class of polymers that exhibit this phenomenon; due to the presence of thermosensitive polypropylene oxide (PPO) repeating unit, they self-assemble into micelles beyond the LCST of this block.<sup>[42]</sup> These ABA-type triblock copolymers made of polyethylene oxide (PEO) and PPO blocks have been extensively investigated since they are widely available in a range of compositions and molecular weights.<sup>[43]</sup> Among the most popular of these copolymers is Pluronic F127, which has a molecular weight of 12,500 Da and is made up of 30% wt PO units and 70% wt EO units.<sup>[44,45]</sup> Notably, Pluronic F127 has been authorized by the Food and Drug Administration (FDA) for several medical applications, including drug delivery.<sup>[46]</sup> When a hydrophobic substance is added, it tends to collect in the hydrophobic PPO core, a behavior that is exacerbated as the temperature rises. A hydrophilic PEO corona is generated to “shield” these areas. As a result, the hydrophobic drug water solubility drastically improves in aqueous solutions, boosting the A.P.I.'s (Active Pharmaceutical Ingredient) bioavailability.<sup>[47]</sup> Despite the fact that Pluronic copolymers cannot be broken down internally, the kidneys typically filter out these systems, which are then eliminated through micturition.<sup>[10]</sup>

Considering all of the above, hyperbranched copolymer, H-[P(OEGMA-co-LMA)] was paired with the linear thermosensitive triblock copolymer, Pluronic F127 to produce mixed micelle nanostructures. This work focuses on the preparation schemes for the formation and stabilization of mixed polymeric nanostructures with interest in studying how varying architecture and composition of the polymer chain combine in terms of self-assembly, as well as for the encapsulation of drugs that exhibit different degrees of solubility.

**Table 1.** Protocol comparison of neat mixed copolymer nanostructures.

Formulation code	$g_H:g_{F127}$	Organic solvent <sup>a)</sup>	Protocol	Dispersion medium	Intensity <sub>90°</sub> [a.u.]	$R_h$ [nm]	PDI
N1	1:1	Ac.	Thin Film	PBS	31 600	101	0.439
N2	1:2	Ac.	Thin Film	PBS	14 354	104 [75%] 25 [22%]	0.507
N3	1:1	Ac.	Co-solvent	PBS	780	16	0.13
N4	1:2	Ac.	Co-solvent	PBS	1439	16	0.226
N5	1:1	Eth.	Thin Film	PBS	19 516	121 [81%] 21 [19%]	0.486
N6	1:1	Eth.	Co-solvent	PBS	711	14	0.111
N7	1:2	Eth.	Co-solvent	PBS	2968	20	0.108

Temperature: 37 °C. <sup>a)</sup>Ac: Acetone, Eth: Ethanol.

## 2. Results

### 2.1. Self-Assembly Studies on Mixed Neat Polymeric Nanostructures in Aqueous Media

#### 2.1.1. Preparation Protocol Comparison

Dynamic light scattering experiments were conducted, to determine the apparent hydrodynamic radius ( $R_h$ ) and the size polydispersity index (PDI) of the self-assembled polymeric nanostructures. The final concentration of H-[P(OEGMA-co-LMA)] in all colloidal systems was  $10^{-3}$  g mL<sup>-1</sup> while different weight ratios (1:1 and 1:2) of each copolymer were investigated. Measurements were obtained in the range of 25–37 °C, to simulate conventional drug conditions and to study Pluronic's F127 influence in the emerging nanostructures as a thermoresponsive element. In the Thin Film protocol, acetone and ethanol were also tested to determine whether the choice of organic solvent in the preparation protocol had an impact on the results. The co-solvent approach was continued with ethanol alone after it was determined that results were similar, considering the fact ethanol is a preferred organic solvent for biomedical applications. PBS or WFI made up the aqueous medium. When  $g_H:g_{F127}$  is mentioned, it refers to the weight ratio of H-[P(OEGMA-co-LMA)] and Pluronic F127 respectively. The results analyzed by the cumulants method and CONTIN algorithm are presented in **Table 1**.

Based on these findings, the thin film protocol was unsuccessful in producing adequate nanostructures. Considering that two populations are visible in all ratios for both organic solvent protocols, it is likely that the self-assembly behavior is affected by Pluronic's thermoresponsive properties (**Figure 1**) since the nano-assemblies are formed in the absence of heating. Additionally, Pluronic mixed micelles (P123/F127) have been successfully synthesized in a similar manner, implying that the hyper-branched copolymer may play an important role in the present outcome.<sup>[48]</sup>

On the other hand, nanostructures that self-assembled using the co-solvent approach displayed low PDI, and  $R_h$  that were between 14 and 20 nm in size, which is well within the range of the nanoscale (1–100 nm).<sup>[49]</sup> The co-solvent approach probably facilitates a smoother transition towards aqueous state assembly while Pluronic is in an elevated hydrophobic condition since the heating temperature for organic solvent elimination is above its LSCT. Monomodal size distributions were observed after the effective mixing of the copolymers and both N6 and N7 formula-

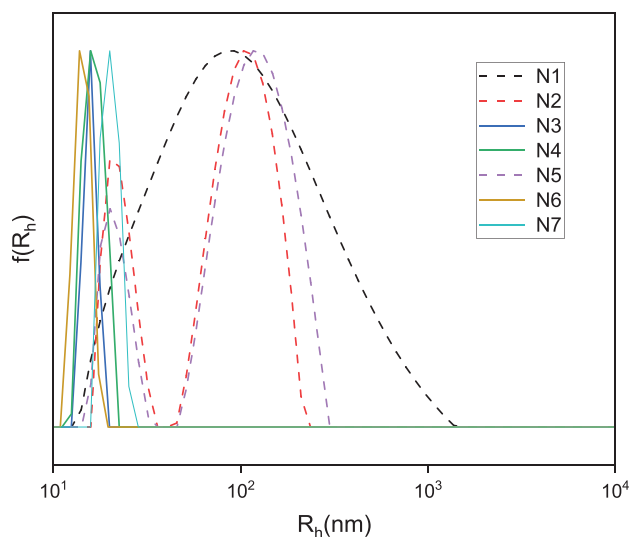


**Figure 1.** Size distributions from CONTIN analysis for the neat mixed copolymer nanostructures. Temperature: 37 °C.

tions outperformed their counterparts generating smaller aggregates. It is interesting to note that for N6 in the heating transition to 37 °C, the intensity increases (612 to 711 Kcps), while regarding PDI values, these aggregates start to form larger structures as the temperature rises and PPO units become more hydrophobic, explaining the PDI shift from 0.032 to 0.111. There are variations between the results of N6 and N7. Presumably, in order to counteract the rise in hydrophobicity, larger structures—both in volume and mass—are produced when the triblock copolymer component is higher. Overall results, including the lack of small-size unimers (0.50–0.69 nm, which correspond to single chains of F127) or aggregates (>50 nm in the case of H-[P(OEGMA-co-LMA)]) are in agreement with the formation of micelles.<sup>[50,51]</sup>

#### 2.1.2. Critical Aggregation Concentration (Cac) Analysis

The critical aggregation concentration (CAC) was examined to assess the ability of copolymers to self-assemble in PBS. When this concentration is reached, the formation of micelles in solutions is thermodynamically preferred.<sup>[52]</sup> These structures tend to disintegrate when distributed out in large volumes, like in blood circulation. An adult human has, on average, 5 liters of blood in circulation, though this amount varies depending on a per-

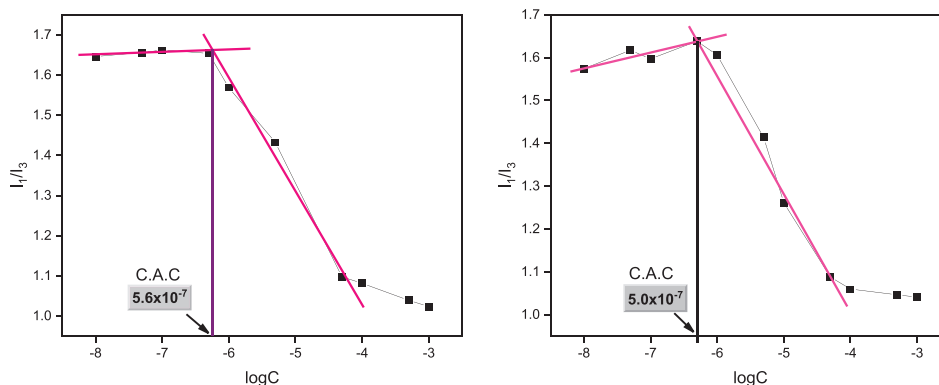


**Figure 2.** CAC determination of mixed copolymer formulations N6 (left) and N7 (right). The aqueous medium was PBS.

son's size, weight, and sex.<sup>[53]</sup> This is troublesome because micelles may abruptly leak into the bloodstream when employed for drug delivery due to micelle disintegration. All of the major advantages of nanocarriers might be hampered by premature drug release, offering results comparable to those of a free drug. The CAC of the nanostructures was determined by fluorescence assay using pyrene as a fluorescent probe. The intensity ratio ( $I_1/I_3$ ) of pyrene excitation spectra is a sensitive indicator of the polarity of its environment. A rise in the hydrophobic moieties indicates that more pyrene will be confined in the aggregates. This approach is predicated on the idea that the pyrene emission spectra will remain constant until the CAC. The disintegration of the micelles, as seen by the high values of  $I_1/I_3$ , results in the release of pyrene molecules into the aqueous environment. The graphs of the concentration versus intensity ratio of the relative first and third vibronic peaks  $I_1/I_3$  are shown in **Figure 2**. At the intersection of two straight lines drawn in the groove of the plateau and stable points, a perpendicular line is drawn, and the value of the logarithmic concentration is defined as the critical aggregation concentration.<sup>[47,54,55]</sup> For colloidal system N6, the CAC value was as low as  $5.6 \times 10^{-7} \text{ g mL}^{-1}$ . N7 demonstrated a more favorable outcome with a value of  $5.0 \times 10^{-7} \text{ g mL}^{-1}$ . Considering Pluronic F127 has a CMC value of  $6.9 \times 10^{-5} \text{ g mL}^{-1}$ <sup>[5]</sup> and H-[P(OEGMA-co-LMA)] has a value of  $2.5 \times 10^{-6} \text{ g mL}^{-1}$ <sup>[36]</sup> both mixed systems resulted in a lower CAC value when compared to their parent copolymers, lending credence to the idea that mixed systems may be superior to their copolymer constituents alone. The increase in hydrophobic moieties is surely contributing to a more stable structure resisting degradation upon dilution. These mixed nanostructures have better stability and the capacity to preserve integrity even under conditions of significant body dilution because of the low CAC values.

### 2.1.3. Zeta Potential ( $\zeta_p$ )

Nanoparticles can be classified into three groups depending on their zeta potential ( $\zeta_p$ ) values, if it is within the range of +10 and  $-10 \text{ mV}$ , it is deemed to be essentially neutral. These structures, however, are regarded as significantly cationic or anionic if their zeta potential falls outside of the  $\pm 30 \text{ mV}$  spectrum. Given that most biological membranes have a negative charge, zeta potential can impede a nanoparticle's ability to pass through

cellular membranes.<sup>[56]</sup> Due to the buffer's high salt content,  $\zeta_p$  measurements were performed in high-purity grade analytical water. Formulations N6 and N7 both registered values of  $-25.3$  and  $-18.8 \text{ mV}$ , respectively. The presence of carboxyl groups on the chain ends of the hyperbranched copolymer is possibly what generates the negative  $\zeta_p$  readings.<sup>[35]</sup> This assumption is amplified by the fact that Pluronic is made up of non-ionic PPO and PEO segments. A study on negatively charged micelles demonstrated that negatively charged chitosan micelles had a 6 times greater capacity for mucus permeation than their positively charged counterparts, demonstrating the necessity of a negative charge for drug delivery applications.<sup>[57]</sup> Another study involving amphiphilic copolymer-based nanoparticles reported that numerous cell lines assimilate cationic nanoparticles more rapidly than negatively charged nanoparticles although they also have a higher potential for cytotoxicity.<sup>[58]</sup>

## 2.2. Self-Assembly Studies on Mixed Drug-Loaded Polymeric Nanostructures in Aqueous Media

### 2.2.1. Particle Size

The capacity of the mixed nanocarriers N6 and N7 to encapsulate curcumin and indomethacin in separate instances was examined, taking into account both the copolymer's biocompatibility and self-assembling behavior. This was done to obtain data on drugs with varying degrees of hydrophobicity. The attempt to encapsulate 20% of curcumin resulted in the drug sedimenting; this drug concentration was probably excessively high for the nanocarrier to sustain colloidal stability. DLS data are collected in **Table 2**.

Curcumin was successfully encapsulated by F127:H-[P(OEGMA-co-LMA)] = 1 and F127:H-[P(OEGMA-co-LMA)] = 2 and attained aqueous solubility (**Figure 3**). It is important to emphasize that each sample had satisfactory outcomes, especially in terms of the size and monodispersity of the emergent mixed structures (**Figure 4**). The hydrophobic drug being tightly packed in the micelles, which enhances the hydrophobic interactions, is most likely to be responsible for this. Prior studies on the encapsulation of hydrophobic substances in Pluronic copolymer micelles found that the inclusion of these drugs increases the radii of the micelles, which is also visible in the present mixed

**Table 2.** DLS data for drug-loaded mixed copolymer nanostructures.

Formulation code	$\text{F}_{127}:\text{H}$	A.P.I. <sup>a)</sup>	Dispersion agent	Temperature [C°]	Intensity <sub>90°</sub>	$R_h$ [nm]	PDI
CUR1	1:1	Cur.	PBS	25	2297	17	0.14
				37	2587	18	0.01
CUR2	1:2	Cur.	PBS	25	4800	27	0.19
				37	4970	29	0.272
IND1	1:1	Ind.	PBS	25	4310	18[49%]	0.351
				37	4470	75[48%]	0.333
						69[49%] 18[50%]	
IND2	1:2	Ind.	PBS	25	1581	22	0.2
				37	1855	19	0.182
IND3	1:1	Ind.	WFI	25	2158	34	0.441
				37	2341	13[48%] 70[51%]	0.419
IND4	1:2	Ind.	WFI	25	2558	36	0.432
				37	2819	15[38%] 97[61%]	0.395

<sup>a)</sup> Cur: curcumin, Ind: indomethacin

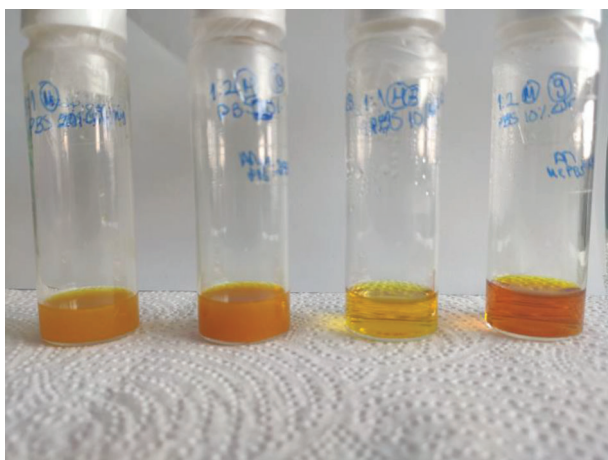


**Figure 3.** Emerged samples of drug loading schemes. From left to right, F127:H-[P(OEGMA-co-LMA)] = 1 injected with 20% wt of curcumin, F127:H-[P(OEGMA-co-LMA)] = 2 injected with 20% wt of curcumin, CUR1, CUR2. The higher amount of drug was unsuccessful in producing stable drug-loaded nanostructures.

systems. This implies that the hydrophobic core of the polymeric nanostructures is where the drug is primarily contained.<sup>[59,60]</sup> This could be because by increasing the hydrophobicity in an aqueous solution with the incorporation of a drug like curcumin, the core of the structure becomes more strongly hydrophobic, necessitating the incorporation of more hydrophilic chains to form the hydrophilic corona as protection around it making the final structure much larger. Additionally, even after the drug was introduced, the formations' radius did not exceed 50 nm, which is required for tumors with minimal permeability. Furthermore, nanoparticles with diameters smaller than 6 nm are swiftly cleared from the body because they may be flushed by the kidneys. Nanocarriers that surpass this cut-off result in a prolongation of the drug's half-life.<sup>[61,62]</sup> F127: H-[P(OEGMA-

co-LMA)] = 1 (CUR1) performed marginally better than the double ratio (CUR2), similar to the neat nanostructures in terms of uniform aggregates. Also, in the case of CUR1, the rise in temperature led to reduced diversity and an increase in mass of the emerging nanostructures as concluded by the increase in the scattered light intensity, which could be attributed to the rise in hydrophobicity. This means that the thermoresponsiveness of Pluronic is still demonstrated in the mixed curcumin-loaded nanostructures.

However, the performance of indomethacin-loaded structures was different. Nearly all formulations included two distinct populations of nanostructures. When measured at body temperature, there is a decrease in the observed radii with the addition of the hydrophobic drug in a manner similar to that observed in indomethacin-loaded Pluronic micelles.<sup>[50]</sup> IND2 yielded structures with favorable properties ( $R_h = 19$  nm and PDI = 0.182). When compared with the mixed nanostructures F127:H-[P(OEGMA-co-LMA)] = 2 loaded with curcumin, although having comparable PDIs, they are smaller in size. To counteract the hydrophobicity of curcumin, Pluronic F127 and other poloxamers typically produce larger micelles with diameters ranging from 20 to 50 nm.<sup>[47,63]</sup> In contrast, a study by Sharma et al. found that indomethacin causes the size of the Pluronic F127 micelles to shrink by 1.1 nm, which is consistent with our findings.<sup>[50]</sup> Additionally, the size and PDI of the newly formed structures appear to be influenced by the suspension agent, as shown by the diverse PBS and WFI values for the structural parameters. Conclusions on the remaining samples should rely on stability studies to provide further context, however.

### 2.2.2. Zeta Potential ( $\zeta_p$ )

$\zeta_p$  is an indicator of colloidal stability. High levels of stability are present in nanoparticles with  $\zeta_p$  values in the region above the absolute value of 30 mV. Colloidal systems with  $\zeta_p$  values of less than +25 mV or more than -25 mV will eventually aggregate.<sup>[64]</sup>

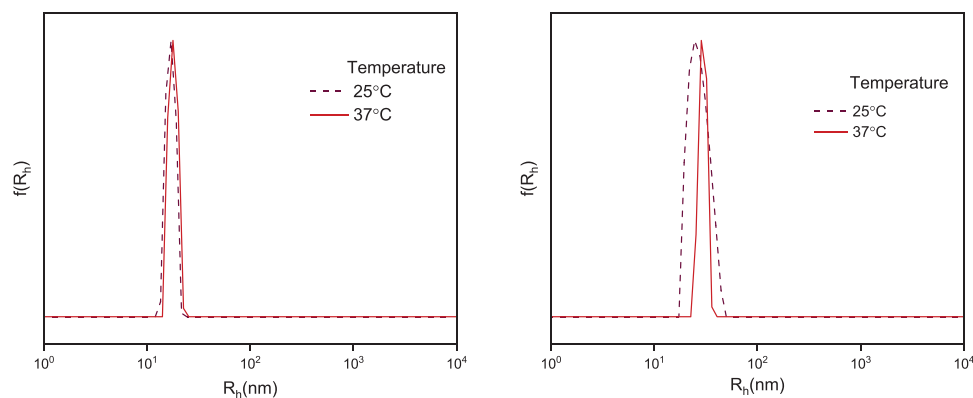


**Figure 4.** Size distributions from CONTIN analysis for formulation CUR1 (left) and CUR2 (right).

**Table 3.**  $\zeta_p$  values for drug-loaded nanostructures dispersed in high-purity grade analytical water.

Mixed loaded nanostructures	$\zeta_p$ [mV]
F127:H-[P(OEGMA-co-LMA)] = 1 10% curcumin	-15.2
F127:H-[P(OEGMA-co-LMA)] = 2 10% curcumin	-2.0
F127:H-[P(OEGMA-co-LMA)] = 1 10% indomethacin	-22.7
F127:H-[P(OEGMA-co-LMA)] = 2 10% indomethacin	-19

The formulations appear to be colloiddally unstable in the majority of cases (Table 3). It is crucial to keep in mind that while colloidal stability is linked to higher  $\zeta_p$  values, the truth is more nuanced. Just as mentioned before  $\zeta_p$  serves as an indicator but is not the sole determining factor. Colloid stability is determined by the sum of van der Waals attractive forces, steric and electrostatic interactions and because of this, stable colloidal suspensions with moderate  $\zeta_p$  and vice versa are not rare. It is worth emphasizing PEGylation, which is known to boost nanoparticle durability while decreasing zeta potential by masking negatively charged nanoparticles because of steric effects originating from the hydrophilic non-ionic PEG chains.<sup>[35,65,66]</sup> The high standard deviation should be the reason for the wide variance between the curcumin-loaded nanostructures. The carboxyl group, as discussed in previous sections, is most likely the source of the negative charge which induces a minor electrostatic repulsion force between the nanostructures. Similar results are obtained from the drug-loaded hyperbranched copolymer aggregates,  $\zeta_p = -18.6$  mV.<sup>[35]</sup> While there is a slight decrease when compared to the neat nanostructures, this is most likely due to the addition of the A.P.I., which acts as a compensating component. The  $\zeta_p$  values of all formulations were negative, which is advantageous for nanomedicine applications. Cationic particles are more prone to causing hemolysis and blood clotting than neutral or anionic particles. Furthermore, positively charged nanoparticles tend to gravitate toward the liver, spleen, and lungs. Also, neutral or slightly negatively charged nanoparticles do not interact with serum proteins boosting the formulation's half-life.<sup>[62,67,68]</sup>

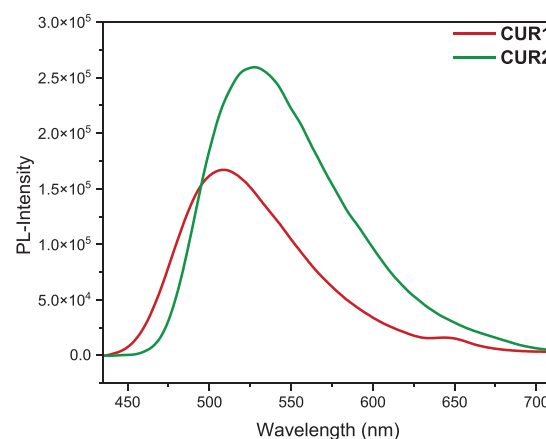


**Figure 5.** FS results of curcumin-loaded mixed polymeric nanostructures dispersed in PBS. [10% curcumin].

### 2.3. Fluorescence Assay

Early detection and intervention are key for many pathological states. Nanoformulations help significantly by assisting in the development of screening techniques that enable the detection of several anomalies in minuscule amounts. As a result, it stands to reason for diagnostic techniques like fluorescence imaging (FI) to make use of the opportunity that nanoparticles present. The use of organic dyes and other conventional probes frequently displays biocompatibility; they lack targeting mechanisms, frequently have minimal absorption, and result in rapid expulsion from the body. Evidently, the photostability capabilities of nanoparticles are far superior to those of molecular probes. Furthermore, nanoparticles are distributed more evenly throughout the body when passive targeting is used as the method of distribution.<sup>[69-73]</sup> Curcumin has been employed in bioimaging research.<sup>[74]</sup> To determine whether the same fluorescent properties persisted after micellization, fluorescence spectroscopy was used. Curcumin excitation wavelength was set at 405 nm. Formulations CUR1 and CUR2 each had a concentration of  $1.0 \times 10^{-4}$  and  $1.5 \times 10^{-4}$  g mL<sup>-1</sup>, respectively. The curcumin's fluorescent properties were still present in the loaded nanostructures (Figure 5), although the result defies the expectation that higher

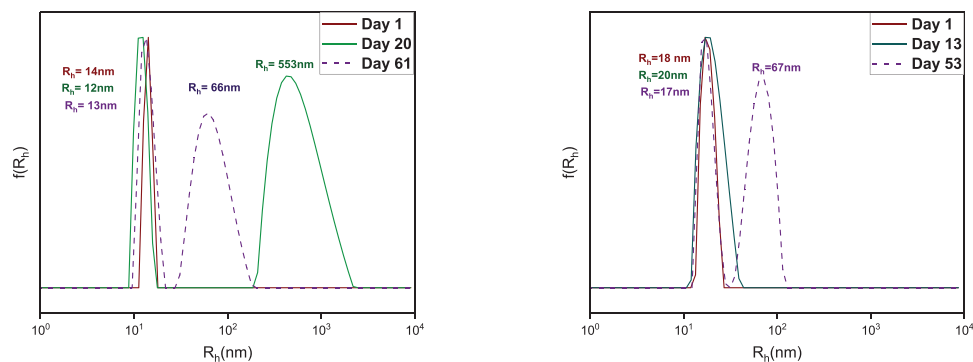


**Figure 6.** Size distributions from CONTIN analysis of formulations N6 (left) and N7 (right) (Temp.:25 °C).

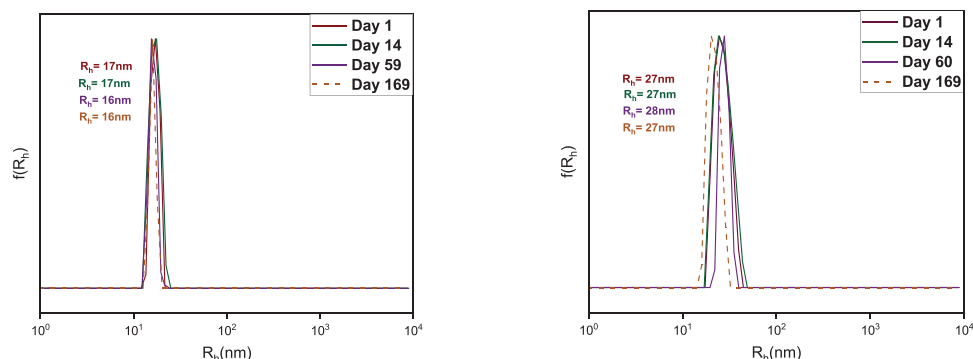


**Figure 7.** Size distributions from CONTIN analysis of formulations CUR1 (left) and CUR2 (right) over 169 days (Temp.: 25 °C).

concentrations would result in higher intensity values. The notion that nanostructures change their morphologies depending on concentration may help to explain the phenomenon. Self-quenching is the term used to describe this transformation. In acetone, curcumin typically peaks at a wavelength of 504 nm. Curcumin 10% in CUR1 and CUR2 both exhibit a minor shift to 507 and 527 nm, accordingly. The hydrophobic interactions between curcumin and the hydrophobic PPO and LMA units of both copolymers were most likely responsible for this shift.<sup>[75]</sup> Overall, curcumin's fluorescence properties were maintained, and water solubility was reached in the loaded nanostructures.

## 2.4. Drug Release

The dialysis method was used to assess the drug quantity that could be released from the polymeric nanostructures. Measurements on CUR1 and CUR2 were conducted over a 26-hour period. When compared to earlier studies of curcumin nanofor-mulations, the hydrophobic dye does not leak into the receptor solution over this time span. There were no peaks detected in the 420 nm range. Curcumin can exhibit a peak at 427 nm and a shoulder at 360 nm in aqueous solutions. The first peak corresponds to the enolic form and the second to the ketonic form.<sup>[76–78]</sup> These findings suggest that the free drug could not escape from the nanocarrier. Additionally, the receptor solution was never significantly tinted, even after the completion of the experiment. Under these circumstances, when compared to the DLS data (as discussed in section 3.5), the nanostructures appear to retain their structure. Considering these results, these mixed

systems could be employed in bioimaging since they show negligible leakage of the photoactive species.

## 2.5. Colloid Stability Studies

The formulations' temporal stability was examined using dynamic light scattering techniques (Figure 6 and 9). With the exception of the dialysis assay, the same stock solution was used to avoid batch-to-batch variability, and it was kept airtight to avoid contamination. The DLS graphs list the various timeframes in which samples were measured (Figure 6–10). In the absence of the hydrophobic drug, the morphology of these nanostructures can change over time. Micelles that rely heavily on hydrophobic interactions to maintain their initial structure stable may develop more thermodynamically stable structures that lack the characteristics required for effective nanocarriers. The development of a new population of nanostructures occurred in both the cases of the organic solvents, acetone and ethanol. The size distribution indicates that the same nanostructures may agglomerate to form larger structures while retaining a sizable portion of the original structures. This discovery might also assist to explain the rise in PDI (N6 PDI: 0.032→0.608→0.420, N7 PDI: 0.262→0.040→0.343). Formulation N7 was able to maintain its consistency with minimal changes in hydrodynamic radii for at least two weeks. The observation that it almost attained monodispersity with this storage time is intriguing. N6 on the other hand at the 20-day mark produced large structures which either rearranged over time or settled on the bottom of the cuvette. The mixed nanostructures containing curcumin displayed adequate

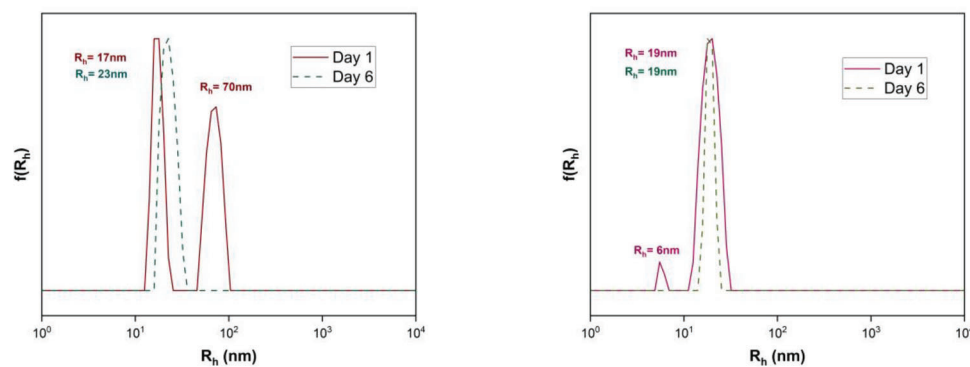


**Figure 8.** Size distributions from CONTIN analysis of formulations IND1 (left) and IND2 (right). Note: Temperature 37 °C.

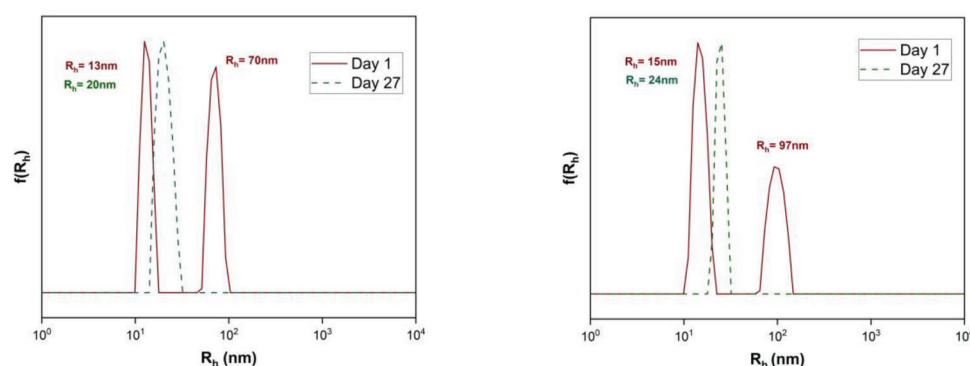


**Figure 9.** Size distributions from CONTIN analysis of IND3 (left) and IND4 (right). Note: Temperature: 37 °C.

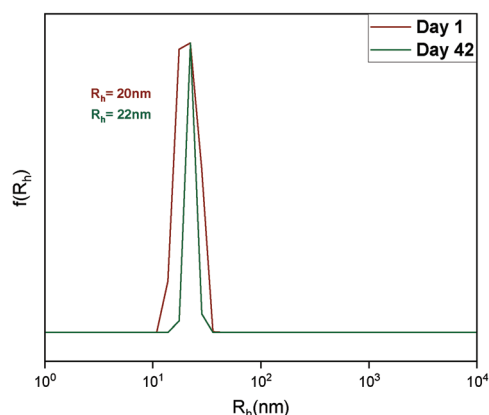


**Figure 10.** Size distributions from CONTIN analysis of CUR2 after dialysis (Temp.:37 °C).

integrity over the course of 169 days. It is evident that the addition of curcumin significantly increased these systems' stability. At the 169-day point, both systems showed acceptable PDI values (PDI CUR1 = 0.128, PDI CUR2 = 0.038). The hyper-branched copolymer demonstrated comparable stability characteristics in water, indicating that this element of the mixed system may have aided in maintaining the system's integrity. Previous studies have established that hydrophobic interactions between Pluronic F127 and curcumin significantly affect storage stability. The hydrophobic methyl group in the PPO chain of the

Pluronic triblock copolymer is the primary site of interaction between the hydrophobic drug and the micelle core. Among the reasons Pluronic F127 is favored over other poloxamers is because it has more hydrophobic interaction sites.<sup>[79,80]</sup> CUR2 was the most durable drug-loaded nanocarrier since it was able to keep the majority of its initial physicochemical properties. As part of the drug release assay, a sample from the dialysis bag was taken. The loaded nanostructures showed sufficient integrity after a week in the dialysis tubing, which lasted over time, as seen in the graph that follows (Figure 10). When compared to the original CUR2 sample, the different hydrodynamic radii could be the result of batch-to-batch variability. The nanostructures conformed to more uniform structures throughout the course of 42 days, with a modest drop in PDI values from 0.168 to 0.117.

The highest structural alterations, however, were observed in the indomethacin-loaded nanostructures. Both sets of systems appear to have taken substantially longer to shift to their preferred assemblies. Given the length of time it took for the nanostructures distributed in water to undergo this transition, salinity appears to have an effect on this transformation. The second ratio of the nanostructures which were dispersed in the PBS buffer already conformed with a more beneficial structure from the beginning, which gives credence to this theory. Narrow unimodal size distributions were detected in all indomethacin formulations. Significant changes in PDI were observed, notably in water dispersions (IND4 PDI: 0.395 → 0.007 and IND3 PDI: 0.419 → 0.09). Sedimentation was not apparent in any of the samples.

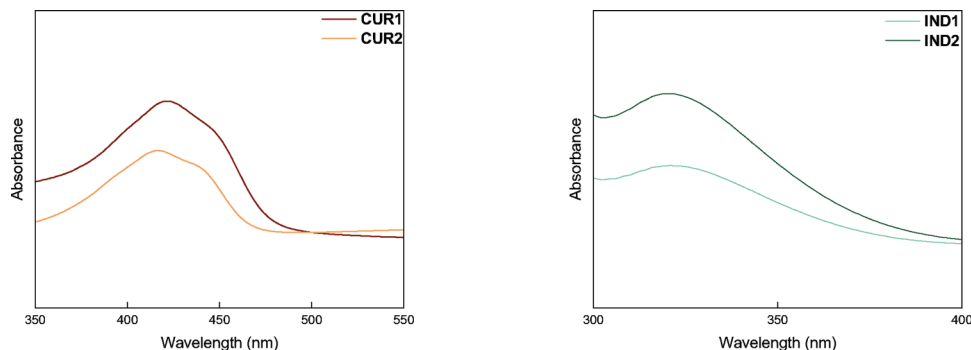


**Figure 11.** UV-vis spectra of the mixed CUR1/CUR10%, CUR2/CUR10%, IND1/IND10%, and IND2/IND10% nanostructures after dilution in PBS.

**Table 4.** DLC and DLE determination based on UV-vis absorption values.

Formulation code	DLC [wt%]	DLE [wt%]
CUR1	2.3	23
CUR2	3.5	35
IND1	1.2	12
IND2	1.8	18

## 2.6. Drug Encapsulation Quantification

UV-vis spectroscopy measurements for formulations CUR1, CUR2, IND1, and IND2 were used to determine the efficacy of the curcumin encapsulation process. **Table 4** presents the findings. **Figure 11** displays UV-Vis spectra of mixed copolymer nanoparticles loaded with curcumin and indomethacin after dilution in PBS. The CUR and IND absorbance was measured at 420 and 320 nm respectively, and the equations below were used to determine the drug loading content (DLC) and drug loading efficiency (DLE) using a calibration curve.

$$\text{DLC (wt\%)} = \frac{\text{weight of loaded drug}}{\text{weight of drug loaded polymer}} \times 100 \quad (1)$$

$$\text{DLE (wt\%)} = \frac{\text{weight of loaded drug}}{\text{weight of initial drug feed}} \times 100 \quad (2)$$

These results demonstrate that the drug was adequately encapsulated and that a higher percentage of the drug can be encapsulated by raising the Pluronic copolymer ratio. This is most likely due to the increase in hydrophobicity of the mixed nanostructures. Notably, it is apparent that this type of nanostructure favors hydrophobic drugs, since a drop in efficiency is seen in the case of indomethacin.

## 2.7. Fetal Bovine Serum Assay

Following the addition of the curcumin-loaded nanoparticles to the FBS/PBS mixed solution, the DLS data were obtained at 25 °C and at a 90° angle. CUR1 and CUR2 were utilized on the 169-day mark, and new formulations (CUR1':  $R_h = 16$  nm and  $PDI = 0.08$  and CUR2':  $R_h = 22$  nm and  $PDI = 0.411$ ) made in accordance

with the same protocol, to achieve a variety of outcomes and replicate the administration of the drug formulation at a later time. The high degree of protein diversity in FBS resulted in a bimodal size distribution with peaks at 2 and 11 nm, respectively. Following the suspension of the curcumin formulation CUR1' in FBS, a new peak of larger-size nanostructures emerges, most likely as a result of opsonization, creating a minor protein corona with serum proteins. As for the rest of the formulations, it is evident that no further aggregation of the existing mixed copolymer systems is taking place. Furthermore, the increase in PDI is due to the presence of unbound proteins. The majority of the curcumin systems exhibit substantial stability in the presence of serum proteins. This is most likely due to the presence of hydrophilic OEGMA side groups and PEO chains of each copolymer which form a hydrophilic crown offering stealth properties to the system. Relevant DLS plots and data can be found in the supporting information file (Table S1 and Figure S1, Supporting Information).

## 2.8. FT-IR Spectroscopy Analysis

An effective approach for verifying the API indomethacin's efficient encapsulation is IR spectroscopy. The FT-IR spectra of loaded and unloaded F127:H-[P(OEGMA-co LMA)] = 1 nanostructures are depicted in **Figure 12**. To provide a standard, neat indomethacin was also examined. The strong peak at  $1104 \text{ cm}^{-1}$  indicates the stretching of the C–O–C ether group. The significant peaks are listed in order from left to right as follows: The prominent peak at  $1700 \text{ cm}^{-1}$  is caused by the functional group of C=O in indomethacin. The medium intensity peak at  $1600 \text{ cm}^{-1}$  is caused by the aromatic C=C stretch present in indomethacin, which can account for the successful encapsulation of indomethacin in the drug-loaded mixed copolymer assemblies. The interactions between the excipient and the drug are to account for the variations in the range of  $1550$  to  $1750 \text{ cm}^{-1}$ . The prominent peak at  $2889 \text{ cm}^{-1}$  is associated with the C–H stretch, which is also visible in Pluronic's IR spectra. C–OH stretch is responsible for the large broad peak at  $3209 \text{ cm}^{-1}$ . There are minor disparities between the two ratios of copolymers, most notably N6 records higher intensity at the mark of the C–OH peak.<sup>[81–83]</sup> FT-IR spectra of N7 can be found in Figure S2 (Supporting Information).

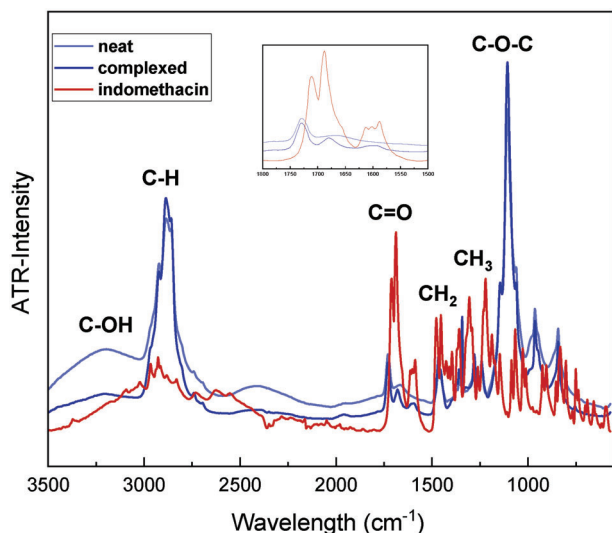


**Figure 12.** FT-IR spectra of F127:H-[P(OEGMA-co LMA)] = 1 in neat and drug complexed form, and neat indomethacin (uncomplexed).

### 3. Discussion

The aim of the present study was to obtain mixed micelles from triblock Pluronic copolymer F127 and H-[P(OEGMA-co LMA)] hyperbranched copolymer with the ability to encapsulate indomethacin and curcumin, two weakly soluble drugs. Pluronic F127 was chosen over other poloxamers due to the significant number and structure of the hydrophobic sites that can interact with hydrophobic drugs. In the realm of mixed micelles, poloxamers are also rising in prominence. H-[P(OEGMA-co LMA)] has hyperbranched units grouped randomly offering versatility. Both cooperate to achieve effective self-assembly, which is caused by the equilibrium between hydrophilic and hydrophobic units. In our previous report on H-[P(OEGMA-co LMA)] systems, smaller hydrodynamic radii are observed after the addition of curcumin. In contrast, the mixed micellar structures follow the norm where the introduction of a hydrophobic drug leads to an increase in the radii of the nano-systems formed.<sup>[59,60]</sup> It is possible that the spatially hindered hyperbranched copolymer segments of higher mass will self-assemble into more numerous and compact nanostructures due to the hydrophobicity of Pluronic, meaning that the hydrophilic segments of each copolymer reach a lower limit to offer a protective barrier to the new core. Moreover, it is important to note that the previously reported H-[P(OEGMA-co LMA)] nanostructures exhibited a higher curcumin encapsulation efficiency, which is likely because the LMA is more accessible and hydrophobic to interact with curcumin.<sup>[35]</sup> However, the significantly lower  $R_h$  sizes and PDI values of the mixed structures discussed here lead us to the assumption that the respective monomodal populations represent a homogeneous dispersion of micelles. Nevertheless, it is challenging to determine with absolute certainty whether such systems are composed of micelles or micelle-like aggregates with many cores, e.g., compound micelles or other similar structures; as a result, additional research on mixed assemblies is needed to support this claim. We can confidently say that the mixed structures are kinetically frozen assemblies rather than equilibrium structures because each method-

ology produced a different set of outcomes. The biocompatibility of the curcumin-loaded nanostructures should be investigated in the future by comparing different biological mediums. It will be necessary to look at the stability of the indomethacin-loaded nanostructures in more detail. This work serves as a useful starting point for discussion and additional research on mixed copolymer nanocarrier systems.

### 4. Conclusion

In this study, mixed copolymer-based nanocarriers, F127:H-[P(OEGMA-co LMA)], were effectively generated utilizing the Thin film and co-solvent approach. Two distinct copolymer weight ratios were used to examine the Pluronic's F127 contribution in the emerging nanostructures. As evidenced by the analysis of the emerging systems, employing dynamic light scattering, each technique was successful in producing mixed copolymer nanostructures. The co-solvent technique resulted in nanocarriers with favorable attributes such as low-size polydispersity indexes and small average micelle hydrodynamic radii. This straightforward method yielded nanostructures that did not surpass 50 nm, making them ideal candidates for drug delivery.

$R_h$  values in neat mixed nanostructures measured from 14 to 20 nm which is above the rapid renal clearance cut-off value. The mixed nanostructures' CAC values were lower compared to aggregates generated under comparable circumstances from the precursor copolymers alone. The capability of the nanocarriers to encapsulate curcumin and indomethacin was examined in separate instances, considering both the copolymer's biocompatible properties and the satisfactory outcomes of the unloaded forms. Curcumin-loaded nanostructures exhibited  $R_h$  values ranging from 17 to 29 nm with exemplary PDI values, while the systems were found to maintain their initial physicochemical characteristics during the 169-day timeframe in PBS. Indomethacin-containing nanosystems required a longer time period to stabilize in a more favorable nanostructure. These systems were measured to be within 19 and 24 nm, with size polydispersity values under 0.02 after the storage period. The findings exemplify the role that hydrophobic compounds contribute in the significantly improved self-organization of these nanostructures. IR spectra provided additional proof that indomethacin was successfully encapsulated. Several interactions between the excipient and the drug were observed in the region of 1550 to 1750  $\text{cm}^{-1}$ . Curcumin's fluorescent properties persisted after encapsulation, as shown by fluorescence spectroscopy. When considering the stability and fluorescence capabilities, the stability assay using dialysis and FS data both showed that the novel curcumin systems had the potential to be used in bioimaging applications.

Curcumin-loaded nanostructures were studied in fetal bovine serum in an effort to simulate the conditions a nanoparticle would experience in the bloodstream. In the majority of formulations, there were significantly minor interactions between the mixed systems and the protein suspension.

This work further adds to a growing corpus of research showing that mixed copolymer systems have the potential to outperform their parent copolymers as drug nanocarriers. The main goal of mixed systems is based on synergism, something that can be witnessed in the size, homogeneity, and CAC values of the emerged systems.

## 5. Experimental Section

**Materials:** Pluronic, a trademark of Sigma, F127 was acquired from Sigma and hyperbranched copolymer H-[P(OEGMA-co-LMA)] 50% wt LMA was synthesized via RAFT polymerization; the exact process was detailed in.<sup>[35]</sup> Curcumin, indomethacin, pyrene, and PBS tablets were procured from Sigma-Aldrich. Water for injection (WFI) was purchased from DEMO ABEE while fetal bovine serum (FBS) was from Gibco.

**Preparation of Neat Mixed Polymeric Nanostructures:** To obtain mixed nanostructures, various approaches were explored. The thin film hydration method and the cosolvent evaporation approach were utilized to produce neat (non-loaded) copolymer nanostructures.

**Preparation of Neat Mixed Polymeric Nanostructures—Thin Film Hydration Method:** Two weight ratios (1:1 and 1:2) of each copolymer (H-[P(OEGMA-co LMA)]-F127) and ethanol or acetone were tested as the organic solvent. Each copolymer was dissolved in the organic solvent; moderate heating was required for Pluronic F127. The systems were then transferred to separate round bottom flasks at the appropriate ratio. The volatile solvent was eliminated by rotary evaporation at room temperature for  $\approx 1$  h depending on the solvent until a clear film was formed on the inner wall of the flask. Phosphate Buffer Saline (PBS, pH = 7.4) was then used to rehydrate the film. The emerged colloidal systems were left to rest overnight before characterization.

**Preparation of Neat Mixed Polymeric Nanostructures—Co-Solvent Method:** The copolymers were dissolved in the organic solvent in a similar manner. The copolymers were combined at the appropriate weight ratio. The organic phase was afterward added rapidly to water or phosphate buffer solution, triggering self-assembly. Heat was then applied via a water bath to eliminate the organic co-solvent. Samples were heated above the boiling point of the organic solvent. The samples were capped and set aside to be characterized the following day.

**Preparation of Drug-Loaded Mixed Polymeric Nanostructures:** The cosolvent method was employed to generate drug-loaded polymeric nanostructures. Theoretical drug encapsulation levels were estimated for each drug in relation to both copolymers for the two formulations of curcumin (10% and 20% wt) and in the case of indomethacin only one concentration was explored (10% wt).

**Dynamic Light Scattering:** The average hydrodynamic radius and size distribution were measured by an ALV/CGS-3 Compact Goniometer System (ALV GmbH, Germany). The analyses were carried out at a fixed angle of 90 degrees using a JDS Uniphase 22 mW He-Ne laser (632.8 nm). A digital ALV-5000/EPP multi-tau correlator with 288 channels was linked to the system. The cumulants method and the CONTIN algorithm were used to examine autocorrelation functions that were taken on average 5 times in a 30-second time frame. To explore Pluronic's influence in terms of thermosensitivity and reproduce actual drug conditions, measurements were taken at three key temperatures ranging from 25 to 37 °C, with a 15 min equilibration between temperatures employing a Polyscience model 9102 bath circulator. All samples were filtered through 0.45  $\mu\text{m}$  hydrophilic PVDF syringe filters.

**Electrophoretic Light Scattering:** The zeta-potential was measured employing a Malvern system (Nano Zeta Sizer) equipped with a 4 mW He-Ne laser tuned to a wavelength of 633 nm. Each value represented the average of 100 successive scans at room temperature.

**Ultraviolet-Visible Spectroscopy:** A Perkin Elmer Lambda 19 spectrometer was used to record the UV-vis spectra in the 200–500 nm region. Three milliliters of each sample were placed in quartz cuvettes for measurement.

**Ultraviolet-Visible Spectroscopy—Drug Release Assay:** The use of mixed micelles as a novel carrier are rendered useless in the case of premature release. To determine if and when these nanocarriers would burst and release the hydrophobic substance curcumin, UV-vis spectroscopy was utilized. Each dialysis tube (3.5 kDa MWCO) was filled with 5 mL of each sample, and the tube was dialyzed against 100 mL of freshly prepared PBS. Given the use of a double-beam UV spectrometer, a reference cuvette containing PBS was set aside and utilized as the reference for all measurements taken on the same day. The samples were set in constant agitation, the receptor solution was supplemented with 3 mL of PBS after each measurement.

**Fluorescence Spectroscopy (FS):** Spectrofluorometer Fluorolog-3 Jobin Yvon-Spex (model GL3–21) was employed to record fluorescence spectra at room temperature.

**Fluorescence Spectroscopy (FS)—Critical Aggregation Concentration (CAC):** The CAC of the nanostructures was determined by fluorescence assay using pyrene as a fluorescent probe. The excitation wavelength employed for the measurements was 335 nm, and the emission spectra were obtained between 355 and 630 nm. Following dilution of freshly prepared mixed nanostructures dispersed in PBS, measurements were done at eight different hyperbranched copolymer concentrations ranging from  $10^{-3}$  to  $10^{-8}$  g mL $^{-1}$ . H-[P(OEGMA-co LMA)]-F127 ratio remained consistent throughout the experiments. The correct quantity ( $1 \mu\text{L mL}^{-1}$ ) of 1 mM pyrene dissolved in acetone was added to each sample, the mixtures were incubated for 12 h in the dark at room temperature to allow the organic solvent to evaporate.

**Fetal Bovine Serum Assay:** Fetal bovine serum is a byproduct of the meat industry. It is widely employed in a wide range of applications in both academic and industrial research. According to proteomic studies, this type of serum contains over 1800 proteins.<sup>[84]</sup> The predominant protein that constitutes between 50% and 60% of the total serum protein is called bovine serum albumin (BSA), and its concentration equates to  $\approx 2.5$  mg mL $^{-1}$ .<sup>[85,86]</sup> Due to its accessibility, FBS is frequently utilized in nanomedicine research to simulate the circumstances which a nanoparticle might encounter in the bloodstream. Incubating nanoparticles in a protein suspension typically results in the formation of a protein corona, which alters the surface morphology of the nanoparticles. These phenomena may impact the durability and elimination mechanisms of nanoparticles in vivo. Therefore, it was helpful to examine the physicochemical characteristics of nanoparticles in such media.<sup>[87,88]</sup> Two protocols were implemented, i) curcumin-loaded mixed copolymer systems in FBS/PBS medium at 1:1 (v/v) and ii) curcumin-loaded mixed copolymer systems in FBS/PBS medium at 1:9 (v/v). In both cases, the protein suspension was used at an FBS:PBS 1:9 (v/v) ratio.

**Infrared Spectroscopy:** The measurements were carried out using a Fourier transform instrument (Bruker Equinox 55, Bruker Optics GmbH) fitted with a single bounce attenuated total reflectance (ATR) diamond accessory (Dura-Samp11R II by SensIR Technologies). Each sample was scanned at a resolution of 2 cm $^{-1}$  over a frequency region of 5000–550 cm $^{-1}$ . The free drug samples were measured in solid form, while the rest were dried using an N $_2$  stream. Each spectrum represents an average of three 100-scan measurements.

## Supporting Information

Supporting Information is available from the Wiley Online Library or from the author.

## Conflict of Interest

The authors declare no conflict of interest.

## Data Availability Statement

The data that support the findings of this study are available from the corresponding author upon reasonable request.

## Keywords

bioimaging, curcumin, drug encapsulation, hyperbranched amphiphilic copolymers, indomethacin, mixed micelles, pluronics

Received: April 13, 2023

Revised: June 15, 2023

Published online: July 10, 2023

- [1] S. Clarysse, J. Brouwers, J. Tack, P. Annaert, P. Augustijns, *Eur. J. Pharm. Sci.* **2011**, *43*, 260.
- [2] R. H. Müller, C. M. Keck, *Eur. J. Pharm. Sci.* **2008**, *34*, S20.
- [3] I. Pepic, J. Lovric, J. Filipovic-Grcic, *Eur. J. Pharm. Sci.* **2013**, *50*, 42.
- [4] A. Parra, I. Jarak, A. Santos, F. Veiga, A. Figueiras, *Materials* **2021**, *14*, 7278.
- [5] Z. Ahmad, A. Shah, M. Siddiq, H.-B. Kraatz, *RSC Adv.* **2014**, *4*, 17028.
- [6] H. Cabral, K. Kataoka, *J. Controlled Release* **2014**, *190*, 465.
- [7] B. Ghosh, S. Biswas, *J. Controlled Release* **2021**, *332*, 127.
- [8] X. Xie, Q. Tao, Y. Zou, F. Zhang, M. Guo, Y. Wang, H. Wang, Q. Zhou, S. Yu, *J. Agric. Food Chem.* **2011**, *59*, 9280.
- [9] N. K. Bhatia, S. Kishor, N. Katyal, P. Gogoi, P. Narang, S. Deep, *RSC Adv.* **2016**, *6*, 103275.
- [10] V. Saxena, M. D. Hussain, *J. Biomed. Nanotechnol.* **2013**, *9*, 1146.
- [11] M. H. M. Leung, H. Colangelo, T. W. Kee, *Langmuir* **2008**, *24*, 5672.
- [12] Y.-J. Wang, M.-H. Pan, A.-L. Cheng, L.-I. Lin, Y.-S. Ho, C.-Y. Hsieh, J.-K. Lin, *J. Pharm. Biomed. Anal.* **1997**, *15*, 1867.
- [13] S. Hagl, A. Kocher, C. Schiborr, N. Kolesova, J. Frank, G. P. Eckert, *Neurochem. Int.* **2015**, *89*, 234.
- [14] H. H. Tonnesen, J. Karlsen, Studies on Curcumin and Curcuminoids VI. Kinetics of Curcumin Degradation in Aqueous Solution.
- [15] M. Bernabé-Pineda, M., Ramírez-Silva, M. Romero-Romo, E. González-Vergara, A. Rojas-Hernández, *Spectrochim Acta A Mol Biomol Spectrosc* **2004**, *60*, 1091.
- [16] C. D. Lao, M. T. Ruffin IV, D. Normolle, S. I. Murray, J. M. Bailey, M. E. Boggs, J. Crowell, C. L. Rock, D. E. Brenner, *BMC Complement Altern Med* **2006**, *6*,
- [17] G. Shoba, D. Joy, T. Joseph, M. Majeed, R. Rajendran, P. Srinivas, *Planta Med.* **1998**, *64*, 353.
- [18] O. P. Katore, S. P. Chary, V. K. Dixit, *J Microencapsul* **1991**, *8*, 1.
- [19] P. Srinath, M. G. Chary, S. P. Vyas, P. V. Diwan, *Pharm Acta Helv* **2000**, *74*, 399.
- [20] S. B. La, T. Okano, K. Kataoka, *J. Pharm. Sci.* **1996**, *85*, 85.
- [21] S. Lucas, *The Pharmacology of Indomethacin Headache* **2016**, *56*, 436.
- [22] B. Maity, A. Chatterjee, S. A. Ahmed, D. Seth, *J. Phys. Chem. B* **2015**, *119*, 3776.
- [23] I. G. Shin, S. Y. Kim, Y. M. Lee, C. S. Cho, Y. K. Sung, *J. Controlled Release* **1998**, *51*, 1.
- [24] G. A. Macones, S. J. Marder, B. Clothier, D. M. Stamilio, *Am. J. Obstet. Gynecol.* **2001**, *184*, 264.
- [25] J. Rogers, L. C. Kirby, S. R. Hempelman, D. L. Berry, P. L. Mcgeer, A. W. Kaszniak, J. Zalinski, M. Cofield, L. Mansukhani, P. Willson, F. Kogan, *Neurology* **1993**, *43*, 1609.
- [26] A. S. Manjappa, P. S. Kumbhar, A. B. Patil, J. I. Disouza, V. B. Patravale, *Crit. Rev. Ther. Drug Carrier Syst.* **2019**, *36*, 1.
- [27] A. B. Ebrahim Attia, Z. Y. Ong, J. L. Hedrick, P. P. Lee, P. L. R. Ee, P. T. Hammond, Y. Y. Yang, *Curr. Opin. Colloid Interface Sci.* **2011**, *16*, 182.
- [28] M. Cagel, F. C. Tesan, E. Bernabeu, M. J. Salgueiro, M. B. Zubillaga, M. A. Moreton, D. A. Chiappetta, *Eur. J. Pharm. Biopharm.* **2017**, *113*, 211.
- [29] I. N. Kurniasih, J. Keilitz, R. Haag, *Chem. Soc. Rev.* **2015**, *44*, 4145.
- [30] C. Gao, D. Yan, *Prog. Polym. Sci.* **2004**, *29*, 183.
- [31] B. I. Voit, A. Lederer, *Chem. Rev.* **2009**, *109*, 5924.
- [32] M. Luzon, C. Boyer, C. Peinado, T. Corrales, M. Whittaker, L. Tao, T. P. Davis, *J Polym Sci A Polym Chem* **2010**, *48*, 2783.
- [33] Yi Shi, X. Cao, S. Luo, X. Wang, R. W. Graff, D. Hu, R. Guo, H. Gao, *Macromolecules* **2016**, *49*, 4416.
- [34] X. Zeng, Y. Zhang, A. M. Nyström, *Biomacromolecules* **2012**, *13*, 3814.
- [35] A. Balafouti, S. Pispas, *Journal of Polymer Science*, *60*, 1931.
- [36] K. Sano, K. Umemoto, H. Miura, S. Ohno, K. Iwata, R. Kawakami, M. Muneane, T. Yamasaki, D. Citterio, Y. Hiruta, T. Mukai, *ACS Appl Polym Mater* **2022**, *4*, 4734.
- [37] J.-F. Lutz, Ö. Akdemir, A. Hoth, *J. Am. Chem. Soc.* **2006**, *128*, 13046.
- [38] O. Nakagawa, N. Fujimoto, T. Nishiura, T. Kitayama, K. Hatada, *Polym. Bull.* **1992**, *29*, 579.
- [39] S. Chen, R. Pieper, D. C. Webster, J. Singh, *Int. J. Pharm.* **2005**, *288*, 207.
- [40] M. P. Ginebra, E. B. Montufar, *Biomedical Foams for Tissue Engineering Applications* **2014**, 281.
- [41] M. Wang, B. Duan, *Encyclopedia of Biomedical Engineering* **2019**, 1–3, 135.
- [42] M. Talelli, W. E. Hennink, *Nanomedicine (Lond)* **2011**, *6*, 1245.
- [43] E. Ruel-Gariépy, J.-C. Leroux, *Eur. J. Pharm. Biopharm.* **2004**, *58*, 409.
- [44] M. Bohorquez, C. Koch, T. Trygstad, N. Pandit, *J. Colloid Interface Sci.* **1999**, *216*, 34.
- [45] S. D. Desai, J. Blanchard, *J. Pharm. Sci.* **1998**, *87*, 226.
- [46] R. Ganguly, S. Kumar, A. Kunwar, S. Nath, H. D. Sarma, A. Tripathi, G. Verma, D. P. Chaudhari, V. K. Aswal, J. S. Melo, *J. Mol. Liq.* **2020**, *314*, 113591.
- [47] R. Basak, R. Bandyopadhyay, *Langmuir* **2013**, *29*, 4350.
- [48] Z. Wei, J. Hao, S. Yuan, Y. Li, W. u Juan, X. Sha, X. Fang, *Int. J. Pharm.* **2009**, *376*, 176.
- [49] S. Devasahayam, *Nanoscience and Nanotechnology in Drug Delivery* **2019**, 477.
- [50] P. K. Sharma, S. R. Bhatia, *Int. J. Pharm.* **2004**, *278*, 361.
- [51] D. A. Chiappetta, G. Facorro, E. Rubin De Celis, A. Sosnik, *Nanomedicine* **2011**, *7*, 624.
- [52] D. Hwang, J. D. Ramsey, A. V. Kabanov, *Adv Drug Deliv Rev* **2020**, *156*, 80.
- [53] R. Sharma, S. Sharma, *Physiology, Blood Volume. StatPearls* **2022**.
- [54] A. v Kabanov, I. R. Nazarova, I. v Astafieva, E. v Batrakova, V. Y. Alakhov, A. A. Yaroslavov, V. A. Kabanov5, *Macromolecules* **1995**, *28*, 2303.
- [55] K. Kalyanasundaram, J. K. Thomas, *J. Am. Chem. Soc.* **1977**, *99*, 2039.
- [56] J. D. Clogston, A. K. Patri, *Methods Mol Biol* **2011**, *697*, 63.
- [57] B. Le-Vinh, N.-M. N. Le, I. Nazir, B. Matuszczak, A. Bernkop-Schnürch, *Int. J. Biol. Macromol.* **2019**, *133*, 647.
- [58] D. Hühn, K. Kantner, C. Geidel, S. Brandholt, I. De Cock, S. J. H. Soenen, P. Rivera\_Gil, J.-M. Montenegro, K. Braeckmans, K. Müllen, G. U. Nienhaus, M. Klapper, W. J. Parak, *ACS Nano* **2013**, *7*, 3253.
- [59] F. U. Vaidya, R. Sharma, S. Shaikh, D. Ray, V. K. Aswal, C. Pathak, *Cancer Rep* **2019**, *2*,
- [60] M. A. Tanase, A. C. Soare, L. M. Ditu, C. L. Nistor, C. I. Mihaescu, I. C. Gifu, C. Petcu, L. O. Cinteza, *Pharmaceutics* **2022**, *14*, 2137.
- [61] A. Albanese, P. S. Tang, W. C. W. Chan, *Annu. Rev. Biomed. Eng.* **2012**, *14*, 1.
- [62] H. Cabral, K. Miyata, K. Osada, K. Kataoka, *Chem. Rev.* **2018**, *118*, 6844.
- [63] D. Dantas Lopes Dos Santos, J. F. Besegato, P. B. G. Melo, J. A. Oshiro Junior, M. Chorilli, D. Deng, V. S. Bagnato, A. N. D. e S. Rastelli, *Photochem. Photobiol.* **2021**, *97*, 1072.
- [64] A. Kumar, C. K. Dixit, *Advances in Nanomedicine for the Delivery of Therapeutic Nucleic Acids* **2017**, 4358.
- [65] S. Bhattacharjee, *J. Controlled Release* **2016**, *235*, 337.
- [66] H. Kouchakzadeh, S. A. Shojaosadati, A. Maghsoudi, E. Vasheghani Farahani, *AAPS PharmSciTech* **2010**, *11*, 1206.
- [67] C. F. Jones, R. A. Campbell, A. E. Brooks, S. Assemi, S. Tadjiki, G. Thiagarajan, C. Mulcock, A. S. Weyrich, B. D. Brooks, H. Ghandehari, D. W. Grainger, *ACS Nano* **2012**, *6*, 9900.
- [68] A. E. Nel, L. Mädler, D. Velegol, T. Xia, E. M. V. Hoek, P. Somasundaran, F. Klaessig, V. Castranova, M. Thompson, *Nat. Mater.* **2009**, *8*, 72009, 8, 543.
- [69] A. Vollrath, S. Schubert, U. S. Schubert, *J. Mater. Chem. B* **2013**, *1*, 1994.
- [70] D. Gyawali, S. Zhou, R. T. Tran, Y. Zhang, C. Liu, X. Bai, J. Yang, *Fluorescence Imaging Enabled Biodegradable Photostable Polymeric Micelles Adv Healthc Mater* **2014**, *3*, 182.

- [71] O. S. Wolfbeis, *Chem. Soc. Rev.* **2015**, *44*, 4743.
- [72] M. J. Ruedas-Rama, J. D. Walters, A. Orte, E. A. H. Hall, *Anal. Chim. Acta* **2012**, *751*, 1.
- [73] K. Li, B. Liu, *Chem. Soc. Rev.* **2014**, *43*, 6570.
- [74] S. Govindaraju, A. Rengaraj, R. Arivazhagan, Y.-S. Huh, K. Yun, *Bioconjug Chem* **2018**, *29*, 363.
- [75] D. Selianitis, S. Pispas, *Polym. Int.*, *70*, 1508.
- [76] A. Fattahi Bafghi, B. F. Haghirosadat, F. Yazdian, F. Mirzaei, M. Pourmadadi, F. Pournasir, M. Hemati, S. Pournasir, A novel delivery of curcumin by the efficient nanoliposomal approach against Leishmania major, **2021**, *51*, 990.
- [77] S. Mondal, S. Ghosh, S. P. Moulik, *J Photochem Photobiol B* **2016**, *158*, 212.
- [78] P. Kumar, S. K. Kandi, S. Manohar, K. Mukhopadhyay, D. S. Rawat, *ACS Omega* **2019**, *4*, 675.
- [79] L. Zhao, J. Du, Y. Duan, Y. a' Zang, H. Zhang, C. Yang, F. Cao, G. Zhai, *Colloids Surf B Biointerfaces* **2012**, *97*, 101.
- [80] A. Sahu, N. Kasoju, P. Goswami, U. Bora, *J. Biomater. Appl.* **2011**, *25*, 619.
- [81] B. Karolewicz, M. Gajda, A. Górniak, A. Owczarek, I. Mucha, *J. Therm. Anal. Calorim.* **2017**, *130*, 383.
- [82] M. Kafetzi, S. Pispas, X. Bao, P. Yao, *Biomedicines* **2020**, *8*, 392.
- [83] D. K. Jain, G. Darwhekar, S. S. Solanki, R. Sharma, *J Pharm Investig* **2013**, *43*, 27.
- [84] G. Gstraunthaler, T. Lindl, J. Van Der Valk, *Cytotechnology* **2013**, *65*, 791.
- [85] M. P. M. Soutar, L. Kempthorne, E. Annuario, C. Luft, S. Wray, R. Ketteler, M. H. R. Ludtmann, H. Plun-Favreau, *Autophagy* **2019**, *15*, 2002.
- [86] H. T. R. Wiogo, M. Lim, V. Bulmus, J. Yun, R. Amal, *Langmuir* **2011**, *27*, 843.
- [87] A. Chroni, T. Mavromoustakos, S. Pispas, *Macromol* **2021**, *1*, 177.
- [88] N. Pippa, E. Kaditi, S. Pispas, C. Demetzos, *Soft Matter* **2013**, *9*, 4073.